Power transfer control within the framework of vehicle-to-house technology

Hicham Ben Sassi, Yahia Mazzi, Fatima Errahimi, Najia Es-Sbai

Laboratory of Intelligent Systems, Georesources and Renewable Energies, Faculty of Sciences and Technology, Sidi Mohamed Ben
Abdellah University, Fez, Morocco

Article Info

ABSTRACT

The emerging vehicle-to-grid (V2G) technology has gained a lot of praise in the last few years following its experimental validation in several countries. As a result, this technology is being investigated for standalone houses under the name of vehicle-to-house (V2H). This latter proposes a two-way power transfer between electric vehicles and isolated houses relying on renewable sources for power supply. In this paper an implementation of the V2H technology is investigated, using the adaptive backstepping control approach for the bidirectional half-bridge and the integral sliding mode control for the direct current to direct current (DC-DC) converter. The robustness of the controllers and their capability to respond to the desired performances were tested using different realistic scenarios. The obtained results yielded, a perfect sinusoidal output voltage with an amplitude of 220 V and a frequency of 50 Hz. This is further been validated by a frequency analysis resulting in a total harmonic distortion (THD) of 0.25%.

Corresponding Author:

Hicham Ben Sassi
Laboratory of Intelligent Systems, Georesources and Renewable Energies, Faculty of Sciences and
Technology, Sidi Mohamed Ben Abdellah University
Box 2202, Fez, Morocco
Email: hicham.1bensassi@gmail.com

1. INTRODUCTION

The instability of the petroleum market and the greenhouse gas emissions of conventional vehicles have inspired the development and vast adoption of electric vehicles [1], [2]. These environmentally friendly transportation tools run on electricity provided by an electric grid instead of fuel. As a result, they are expected to play a major role in meeting global goals on climate change. Nevertheless, the increasing power demand by electric vehicles (EVs) is expected to jeopardize the stability of the electrical grids if not controlled properly, resulting in a voltage dip, or line and transformer overloading [3]. In their quest to resolve these hurdles, Kempton *et al.* proposed a new utilization of the EV, relying on vehicle-to-grid (V2G) technology, as described in [4]. This latter allows the EVs to provide power back to the grid within the context of smart grids [5]. Due to their intriguing characteristics, including substantial storage capacity and tolerance for frequent power fluctuations, EVs are excellent candidates for this task [6], [7].

This paper proposes an EV home integration using vehicle-to-house technology (V2H) [8]. In contrast with V2G, V2H is mostly deployed for homes without access to an electrical grid but rather relies on renewable energy sources to fulfill their electricity requirements. As result, the EV could be used to support the battery storage units of the standalone home in case of an emergency, such as heavy machinery operation, or a shortage in photovoltaic (PV) production. The V2H setup adopted in this paper is illustrated in Figure 1. It consists of a PV system, a battery storage unit, and an EV, in addition to the bidirectional direct current to direct current (DC-DC) converter, and the direct current to alternating current (DC-AC) inverter.

The power transfer rate between the EV and the house within the framework of V2H can vary significantly depending on the connected loads, the PV production, and the state of charge of the storage systems [9]. As a result, robust control of the bidirectional power converters (DC-DC and DC-AC) is crucial, to supply the required power regardless of the encountered scenario. In this regard, several control strategies were proposed for the adopted buck-boost converter. The robustness characteristic of an adaptive sliding mode based controller (SMC) was investigated in [10], for a SEPIC-Zeta converter. Furthermore, in [11], the authors presented a Lyapunov-based hysteric controller to manage the power flow of a bidirectional buck-boost converter. This latter is connected between the DC-bus and the main battery storage of an EV. In [12], a hysteretic-modulation-based controller is designed based on the SMC technique to control a versatile buck-boost converter for photovoltaic application.
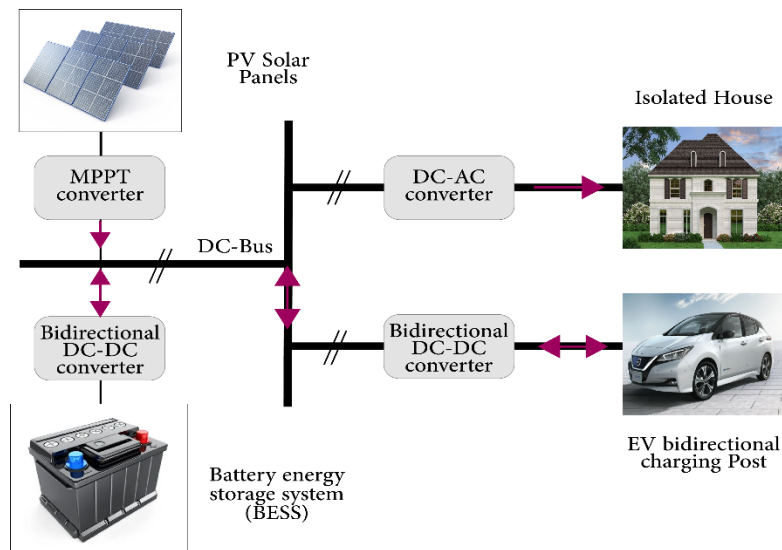

Figure 1. V2H structure with a PV system

In this work, the integral sliding mode (ISM) strategy is suggested to control the amount of power exchanged between the isolated house and the EV. In contrast to its conventional predecessor [13], the ISM control incorporates an integral term in its sliding surface, which enables the integral sliding mode control (ISMC) to avoid the reaching phase. Thus resulting in a quicker convergence time [14], [15].

Given that injecting power into the house is the key characteristic of the V2H technology, therefore, appropriate control of the full-bridge inverter transforming the DC power to a convenient AC output is crucial. In the literature, several linear controllers were proposed to oversee the power transfer of grid-tied inverters [16], [17]. Nonetheless, the limitations associated with linear controllers in terms of stability under sudden load variations, render their use inadvisable in our application. To overcome these issues, nonlinear approaches such as the sliding mode control [18], [19], the fuzzy logic control [20], the predictive control [21], and the backstepping control [22], have been reported in the literature. Such control schemes have proven their superiority, in terms of output stability, tracking performances, and transient response [18]. Based on a comparative analysis conducted in [20], the performances of the backstepping approach were praised over the SMC for the inverter. Accordingly, this paper associates an adaptive approach with the conventional backstepping controller to further enhance its efficiency.

The layout of the rest of this paper is given as: section 2 presents the research method which deals with the modeling of both power converters as well as the design process of the integral sliding mode and the adaptive backstepping control approaches. Followed by a presentation and discussion of the obtained simulation results in section 3. Finally, this paper ends with a conclusion.

2. RESEARCH METHOD

To accurately control the power transfer, two main requirements are needed. these latter are an accurate mathematical model of both power converters, and a delicate design of the control schemes so as to impose the required behavior on the converters. These requirements are addressed in the following sections.

2.1. Bidirectional DC-DC converter

Being that the V2H technology requires a two-way power transfer, the buck-boost converter in Figure 2 is adopted. The operating mode of the converter is imposed by the power needs of the standalone house and the EV battery state of charge (SoC) [23], [24]. When the PV solar panels production exceeds the power needs of the house, and the EV is not fully charged, the converter lowers the voltage so as to charge the EV battery, thus, functioning as a buck power converter. This energy can be used later to power the house in case the PV production is insufficient due to bad weather. In such a scenario the converter elevates the voltage delivered by the EV to equal that of DC bus, hence operating in boost mode. The obtained DC voltage can then be converted to an AC voltage suitable to power the household equipment using the appropriate DC-AC inverter.
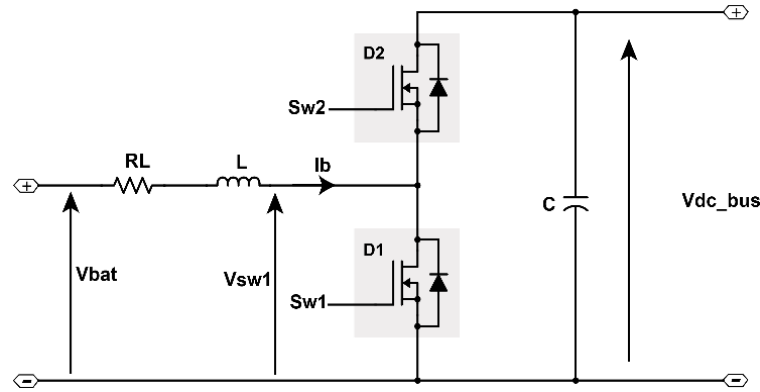
Figure 2. 2sw buck-boost converter

Being that the adopted control schemes in this paper are all model-based. This section provides a mathematical model of the converter in Figure 2 using the dynamic state-space equations which are derived from analyzing the off-state and on-state of the transistors.
− Boost mode

$$V_{Sw1} = (1 - S_{w1})V_{dc} \tag{1}$$

$$\frac{di_b}{dt} = -\frac{R_L i_b}{L} + \frac{V_b}{L} - \frac{V_{Sw1}}{L} \tag{2}$$

$$\frac{di_b}{dt} = -(1 - S_{w1})\frac{V_{dc}}{L} - \frac{R_L i_b}{L} + \frac{V_b}{L} \tag{3}$$

$$\frac{dV_{dc}}{dt} = \frac{i_{dc}}{C} = \frac{i_b(1 - S_1)}{C} \tag{4}$$

− Buck mode

$$V_{Sw1} = S_2 V_{dc} \tag{5}$$

$$\frac{di_b}{dt} = -S_{w2}\frac{V_{dc}}{L} - \frac{R_L i_b}{L} + \frac{V_b}{L} \tag{6}$$

$$\frac{dV_{dc}}{dt} = S_{w2}\frac{i_b}{C} \tag{7}$$

Since the converter operates in both buck and boost modes, an averaged state-space representation is developed based on the equations presented above:

$$\begin{pmatrix} \dot{x}_1 \\ \dot{x}_2 \end{pmatrix} = \begin{pmatrix} \frac{di_b}{dt} \\ \frac{dV_{dc}}{dt} \end{pmatrix} = \begin{pmatrix} \frac{-R_L}{L} & -\frac{K(1-S_{w1})+(1-K)S_{w2}}{L} \\ \frac{K(1-S_{w1})+(1-K)S_{w2}}{C} & 0 \end{pmatrix} \begin{pmatrix} i_b \\ V_{dc} \end{pmatrix} + \begin{pmatrix} \frac{1}{L} \\ 0 \end{pmatrix} V_b + d \tag{8}$$

Let $S_{WG} = K(1 - S_{w1}) + (1 - K)S_{w2}$.

$$\begin{pmatrix} \dot{x}_1 \\ \dot{x}_2 \end{pmatrix} = \begin{pmatrix} \frac{di_b}{dt} \\ \frac{dV_{dc}}{dt} \end{pmatrix} = \begin{pmatrix} \frac{-R_L}{L} & -\frac{S_{WG}}{L} \\ \frac{S_{WG}}{C} & 0 \end{pmatrix} \begin{pmatrix} i_b \\ V_{dc} \end{pmatrix} + \begin{pmatrix} \frac{1}{L} \\ 0 \end{pmatrix} V_b + d \tag{9}$$

Since no model is perfect, the constrained uncertainties are represented by d in the state-space model. It is chosen to take into consideration model parameter errors of 10% magnitude, including R_L, L and C.

2.2. Integral sliding mode control

The ISMC is an enhanced version of the conventional SMC developed by Utkin [25]. This type of controller produces switching control signals that force the system to stay on a specified sliding surface (S), where the stability of the system is assured. In an attempt to eliminate the reaching phase of the conventional SMC and thus enhance the response time of the controller, an integral term is incorporated into the aforementioned sliding surface which resulted in the ISMC [26]. The design process of this latter is as:
- First, the switching function (S), often known as the integral sliding surface, is defined.
- Secondly, a control law that attracts the system state towards the sliding surface (S) is designed. This control law must guarantee that the direction of motion is always towards S as well as the system's stability [27].

The sliding surface used in this research is given in (10). The choice of S is based on the fact that the exchanged power between the DC-bus and the EV is controlled via the charge/discharge current since the DC bus voltage is maintained constate.

$$S = (e) + \mathbb{I} \int_0^t e \, dt \tag{10}$$

$$e = x_1 - I_{bref} \tag{11}$$

where x_1 is the EV battery's current, e is the mismatch between this latter and the reference value (I_{bref}), and $\mathbb{I}$ is a constant gain. The derivative of the sliding surface S is computed as presented in (13), so as to have access to the control signal S_{WG}.

$$\dot{S} = \dot{x}_1 + \mathbb{I}(x_1 - I_{bref}) \tag{12}$$

$$\dot{S} = -S_{WG}\frac{V_{dc}}{L} + x_1(\mathbb{I} - \frac{R_L}{L}) + \frac{V_b}{L} - KI_{bref} \tag{13}$$

Following the design of S, the second step is to develop a control law that forces the states of the system to converge toward S while guaranteeing the system's stability. As a result, the appropriate control law that can satisfy these two demands is composed of two parts as presented in (14).

$$u = S_{WG} = u_{eq} + u_n \tag{14}$$

where u_{eq} is the equivalent control, which ensures the insensitivity of the feedback system to disturbances once on the sliding surface. To accomplish this, u_{eq} is set so as to eliminates the impact of known parameters on the converter's performance. On the other hand, the nonlinear discontinuous control u_n is devoted to cancel the effects of uncertainties and external disturbances. Being that the equivalent control (u_{eq}) is only effective once on the sliding surface, its value is computed as (15) and (16).

$$\dot{S} = 0 \ll = \gg \dot{S} = -u_{eq}\frac{V_{dc}}{L} + x_1\left(\mathbb{I} - \frac{R_L}{L}\right) + \frac{V_b}{L} - \mathbb{I}I_{bref} = 0 \tag{15}$$

$$u_{eq} = \frac{L}{V_{dc}}(x_1\left(\mathbb{I} - \frac{R_l}{L}\right) - \mathbb{I}I_{bref} + \frac{V_b}{L}) \tag{16}$$

The discontinuous control (u_n) is set to always ensures a sliding motion on the predefined dynamics (S) in spite of uncertainties, and by doing so, it secures the controller stability. As a result, the expression of the control u_n is derived using the Lyapunov stability theory as presented in (17) and (18).

$$V = \frac{1}{2}S^2 \tag{17}$$

$$\dot{V} = \dot{S}S = S(-u_{eq}\frac{V_{dc}}{L} - u_n\frac{V_{dc}}{L} + \left(\mathbb{T} - \frac{R_L}{L}\right)x_1 + \frac{V_b}{L} - \mathbb{T}I_{bref} + d) \tag{18}$$

For a controller to be asymptotically stable $\dot{V}$ must be negative, however, $\dot{V} < -K|S|$ is required to force a finite asymptotic convergence. Based on this new constraint as well as the expression of u_{eq} in (16), u_n can be derived from (18) as (19).

$$\dot{V} = S\left(-u_n\frac{V_{dc}}{L} + d\right) \tag{19}$$

where

$$u_n = Ksign(S) \tag{20}$$

$$\dot{V} < 0 \ll=\gg K > d\frac{L}{V_{dc}} \tag{21}$$

The output control signal of the ISMC is designed by joining the two control signals u_n and u_{eq}.

$$u_{12} = \frac{L}{V_{dc}}(\left(\mathbb{T} - \frac{R_L}{L}\right)x_1 + \frac{V_b}{L} - \mathbb{T}I_{bref}) + Ksign(S) \tag{22}$$

2.3. Bidirectional DC-AC inverter control

The power inverter investigated in this section is the full bridge illustrated in Figure 3. It consists of 4 controllable MOSFET transistors, associated with 4 diodes enabling the inverter to operate in a bidirectional power flow. Alongside a low-pass harmonic filter LC that smooth's the output voltage, resulting in a sinusoidal waveform, thus, enhancing the power quality. Furthermore, the LC filter eliminates the switching frequency and protects the inverter from the transients [28]. The inverter supplies an AC load representing either, an electrical grid or the electric equipment in a standalone house.
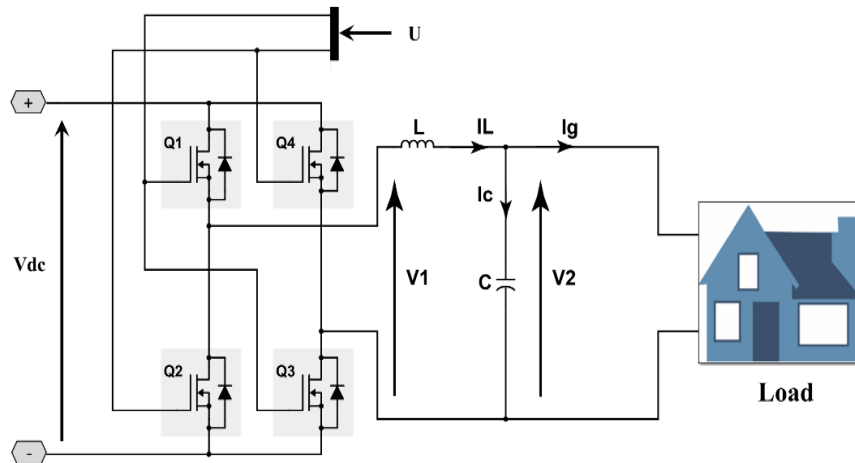

Figure 3. Full bridge inverter

The transforming process of DC to AC is achieved by applying a control signal to the gates of the inverter. Depending on the activation states of each transistor, the output voltage V_1 alternates between $+V_{DC}$, 0, and $-V_{DC}$. The combination of all states results in a rectangular waveform V_1 with an amplitude of $|V_{DC}|$.

Most power inverters are associated with controllers that enforce the desired performances, by acting on their switching transistors. As a result, in this paper, the full-bridge inverter is controlled with PWM based on a backstepping control scheme. Since backstepping is a model-based control strategy, a mathematical model of the power inverter is constructed as:

By applying the Kirchhoff's current law (KCL) and Kirchhoff's voltage law (KVL), the voltage across the capacitor C as well as the inductance's current, evolve following (23) and (24) respectively.

$$C \frac{dV_C}{dt} = C \frac{dV_2}{dt} = I_L - I_g \tag{23}$$

$$L_F \frac{dI_L}{dt} = V_1 - V_2 \tag{24}$$

The output voltage V_1 (prior to the LC filter) is expressed as a function of the switching signal as (25).

$$V1 = Vdc(Sh - Sl) \tag{25}$$

where $Sh = Q1 * Q4$ and $Sl = Q2 * Q3$.

$$L_F \frac{dI_L}{dt} = Vdc(Sh - Sl) - V_2 \tag{26}$$

In control theory, the parameter to be controlled must appear in the state space representation of the plant, as a result, the output voltage across the capacitor V_2 as well as the inductor's current I_L are selected as state variables X_1 and X_2 respectively.

$$\dot{x}_1 = \frac{x_2}{C} - \frac{I_g}{C} \tag{27}$$

$$\dot{x}_2 = \frac{V_{dc}u}{L_F} - \frac{x_1}{L_F} \tag{28}$$

where the control law u is defined as (29) and (30).

$$u = (Sh - Sl) \tag{29}$$

$$\begin{bmatrix} \dot{x}_1 \\ \dot{x}_2 \end{bmatrix} = \begin{bmatrix} 0 & \frac{1}{C} \\ \frac{1}{L_F} & 0 \end{bmatrix} \begin{bmatrix} x_1 \\ x_2 \end{bmatrix} + \begin{bmatrix} 0 \\ \frac{V_{dc}}{L_F} \end{bmatrix} u + \begin{bmatrix} \frac{1}{C} \\ 0 \end{bmatrix} I_g \tag{30}$$

2.4. The adaptive backstepping control approach

Backstepping is a recursive control approach, applied to complex nonlinear systems with triangular state-space representation. In such systems, the control law appears in the nth state, and the desired state can only be controlled via another state of the plant. Backstepping is based on the decomposition of a high-order system into a set of reduced-order subsystems easy to control. The output of each subsystem is injected into the following subsystem as a virtual control law. The global control law is designed using the Lyapunov stability theory.

For the adaptive backstepping approach, the controller gains are recursively adjusted depending on the inverter's behavior. Thus, enhancing the accuracy of the conventional controller. Generally, backstepping is adopted for systems where the desired state can only be controlled via another state of the plant, making it suitable for the inverter, since the output voltage can only be controlled via the output current. The motivation of the control is to establish a sinusoidal output, that is coordinated with the voltage level and frequency of the grid and the electrical equipment of the stand-alone house.

The design process of the backstepping begins by defining the tracking dynamics. Accordingly, the mismatch between the output voltage of the inverter and the reference voltage is defined as (31).

$$e_{b1} = V_{2ref} - x_1 \tag{31}$$

The Lyapunov function that can guarantee the subsystem's stability while designing a virtual control law that nullifies e_{b1} is as:

$$V_1 = \frac{1}{2} e_{b1}^2 \tag{32}$$

Similar to the SMC, the Lyapunov stability theory states that for a positive definite function V_1, the subsystem is asymptotically stable if the derivative of V_1 is strictly negative, as a result:

$$\dot{V}_1 < 0 \leftrightarrow e_{b1}\dot{e}_{b1} < 0 \tag{34}$$

However, for finite-time convergence, zero is replaced with a small quantity.

$$\dot{e}_{b1} = \dot{V}_{2ref} - \dot{x}_1 \tag{35}$$

$$\dot{e}_{b1} = \dot{V}_{2ref} - \frac{x_2}{C} + \frac{I_g}{C} \tag{36}$$

$$\dot{V}_1 = e_{b1}\left(\dot{V}_{2ref} - \frac{x_2}{C} + \frac{I_g}{C}\right) = -K_{b1}e_{b1}^2 \tag{37}$$

The virtual control x_{2des} that substantiates (34) and (37) is then constructed as (38) and (39).

$$e_{b1}\left(\dot{V}_{2ref} - \frac{x_{2des}}{C} + \frac{I_g}{C}\right) = -K_{b1}e_{b1}^2 \tag{38}$$

$$x_{2des} = C\left(\dot{V}_{2ref} + \frac{1}{C}I_g + K_{b1}e_{b1}\right) \tag{39}$$

The second step is to form the appropriate control law u that ensures the convergence of x_2 towards x_{2des}. To this end, the mismatch e_{b2} is defined as (40) and (41).

$$e_{b2} = x_{2des} - x_2 \tag{40}$$

$$x_2 = x_{2des} - e_{b2} \tag{41}$$

Replacing x_2 in (37) by its expression in (41) as well as x_{2des} by its expression in (39) yields:

$$\dot{V}_1 = e_{b1}\dot{e}_{b1} = e_{b1}\left(\dot{V}_{2ref} + \frac{e_{b2}}{C} - \frac{x_{2des}}{C} + \frac{I_g}{C}\right) \tag{42}$$

$$\dot{V}_1 = e_{b1}\dot{e}_{b1} = e_{b1}\left(\dot{V}_{2ref} + \frac{e_{b2}}{C} - \dot{V}_{2ref} - \frac{I_g}{C} - K_{b1}e_{b1} + \frac{I_g}{C}\right) \tag{43}$$

$$\dot{e}_{b1} = \frac{e_{b2}}{C} - K_{b1}e_{b1} \tag{44}$$

The global Lyapunov function V_G that ensures the stability of the entire system is defined as (45) and (46).

$$V_G = V_1 + V_2 = \frac{1}{2}e_{b1}^2 + \frac{1}{2}e_{b2}^2 \tag{45}$$

$$\dot{V}_G = \dot{V}_1 + \dot{V}_2 = e_{b1}\dot{e}_{b1} + e_{b2}\dot{e}_{b2} \tag{46}$$

where

$$\dot{e}_{b2} = \dot{x}_{2des} - \frac{V_{dc}u}{L_F} + \frac{x_1}{L_F} \tag{47}$$

$$\dot{x}_{2des} = C\left(\ddot{V}_{2ref} + \frac{1}{C}\dot{I}_g + K_{b1}\dot{e}_{b1}\right) \tag{48}$$

$$\dot{V}_G = e_{b1}\dot{e}_{b1} + e_{b2}[C\left(\ddot{V}_{2ref} + \frac{1}{C}\dot{I}_g + K_{b1}\dot{e}_{b1}\right) - \frac{V_{dc}u}{L_F} + \frac{x_1}{L_F}] \tag{49}$$

The control law u that is fed to the PWM generator is derived by setting $\dot{V}_G$ as in (50), and substituting $\dot{e}_{b1}$ by its expression in (44).

$$\dot{V}_G = -K_{b1}e_{b1}^2 - K_{b2}e_{b2}^2 \tag{50}$$

$$\frac{1}{C}e_{b1} + C\left(\ddot{V}_{2ref} + \frac{1}{C}\dot{I}_g + K_{b1}\dot{e}_{b1}\right) - \frac{V_{dc}u}{L_F} + \frac{x_1}{L_F} = -K_{b2}e_{b2} \tag{51}$$

$$u = \frac{L_F}{V_{dc}}\left(\frac{1}{C}e_{b1} + \dot{I}_g + CK_{b1}\dot{e}_{b1} + C\ddot{V}_{2ref} + \frac{1}{L_F}x_1 + K_{b2}e_{b2}\right) \tag{52}$$

By setting K_{b1} and K_{b2} as positive values, the tracking error of both states is forced to zero. Henceforward, the inverter produces an output voltage identical to the reference. To avoid the time-consuming process of searching for the exact values of the constants gains K_{b1} and K_{b2}, an adaptive approach is considered. The new proposed control law containing the adaptive gains is given in (53).

$$u = \frac{L_F}{V_{dc}}\left(\frac{1}{C}e_{b1} + \dot{I}_g + C\hat{K}_{b1}\dot{e}_{b1} + C\ddot{V}_{2ref} + \frac{1}{L_F}x_1 + \hat{K}_{b2}e_{b2}\right) \tag{53}$$

$$\dot{\hat{K}}_{bi} = \begin{cases} \mu_i e_{bi}^2 & if\ e_{b_i} > \lambda_i \\ 0 & otherwise \end{cases} \qquad for\ i = 1\ and\ 2 \tag{54}$$

The expression of the adaptive gains is derived using the Lyapunov stability theory. In this regard, the new Lyapunov function becomes.

$$V_{Ad} = \frac{1}{2}e_{b1}^2 + \frac{1}{2}e_{b2}^2 + \frac{\tilde{K}_1^2}{2\mu_1} + \frac{\tilde{K}_2^2}{2\mu_2} \tag{55}$$

$$\begin{cases} \tilde{K}_1 = K_{b1} - \hat{K}_{b1} \\ \tilde{K}_2 = K_{b2} - \hat{K}_{b2} \end{cases} \tag{56}$$

where $\tilde{K}_1$ and $\tilde{K}_2$ are the mismatch between the real and estimated values of the backstepping gains. Seeing that K_{b1} and K_{b2} have a slow variation rate, they can be considered constant in a small-time interval. Thus, the derivative of V_{Ad} can be expressed as (57).

$$\dot{V}_{Ad} = -\hat{K}_{b1}e_{b1}^2 - \hat{K}_{b2}e_{b2}^2 - \frac{\tilde{K}_1(\dot{\hat{K}}_{b1})}{\mu_1} - \frac{\tilde{K}_2(\dot{\hat{K}}_{b2})}{\mu_2} \tag{57}$$

At this stage the estimated value of $\hat{K}_{b1}$ and $\hat{K}_{b2}$ are not yet known, as a result, $\hat{K}_{b1}e_{b1}^2$ and $\hat{K}_{b2}e_{b2}^2$ cannot be declared positive. To overcome this, $\hat{K}_{b1}$ and $\hat{K}_{b2}$ are substituted in (57) by their expressions in (58):

$$\begin{cases} \hat{K}_{b1} = K_{b1} - \tilde{K}_1 \\ \hat{K}_{b2} = K_{b2} - \tilde{K}_2 \end{cases} \tag{58}$$

$$\dot{V}_{Ad} = -K_{b1}e_{b1}^2 - K_{b2}e_{b2}^2 - \tilde{K}_1(-e_{b1}^2 + \frac{\dot{\hat{K}}_{b1}}{\mu_1}) - \tilde{K}_2(-e_{b2}^2 + \frac{\dot{\hat{K}}_{b2}}{\mu_2}) \tag{59}$$

By replacing $\dot{\hat{K}}_{b1}$ and $\dot{\hat{K}}_{b2}$ by their corresponding expression in (54), the derivative of the Lyapunov function V_{Ad} becomes negative. Henceforward, the system is stable.

$$\dot{V}_{Ad} = -K_{b1}e_{b1}^2 - K_{b2}e_{b2}^2 \tag{60}$$

3. SIMULATION AND RESULTS DISCUSSION

This section aims to evaluate the performances of the adaptive backstepping control strategy applied to the power inverter. This includes the convergence time, voltage, and frequency stability, as well as the total harmonic distortion (THD) of the output voltage. To this end, the MATLAB/Simulink model in Figure 4 is constructed. It consists of a standalone house with a PV plant and battery storage system as well as a bidirectional EV charging station. For this study, the output power of both the PV plant and battery storage system is considered to be zero. Accordingly, the power requirements of the house must be provided by the EV using the aforementioned power converter and control schemes. The electrical and control parameters adopted in this section are listed in Table 1.

Given that the voltage level and frequency required by most house equipment are 220 V and 50 Hz respectively, the reference voltage profile in Figure 5 is adopted in this paper. It is a sinusoidal waveform with a voltage level of 220 V and 50 Hz frequency. Initially, this profile is used to investigate the performances of the adopted control schemes in supplying a stable load of 6 KVA. The obtained simulation results are illustrated in Figures 6 and 7.
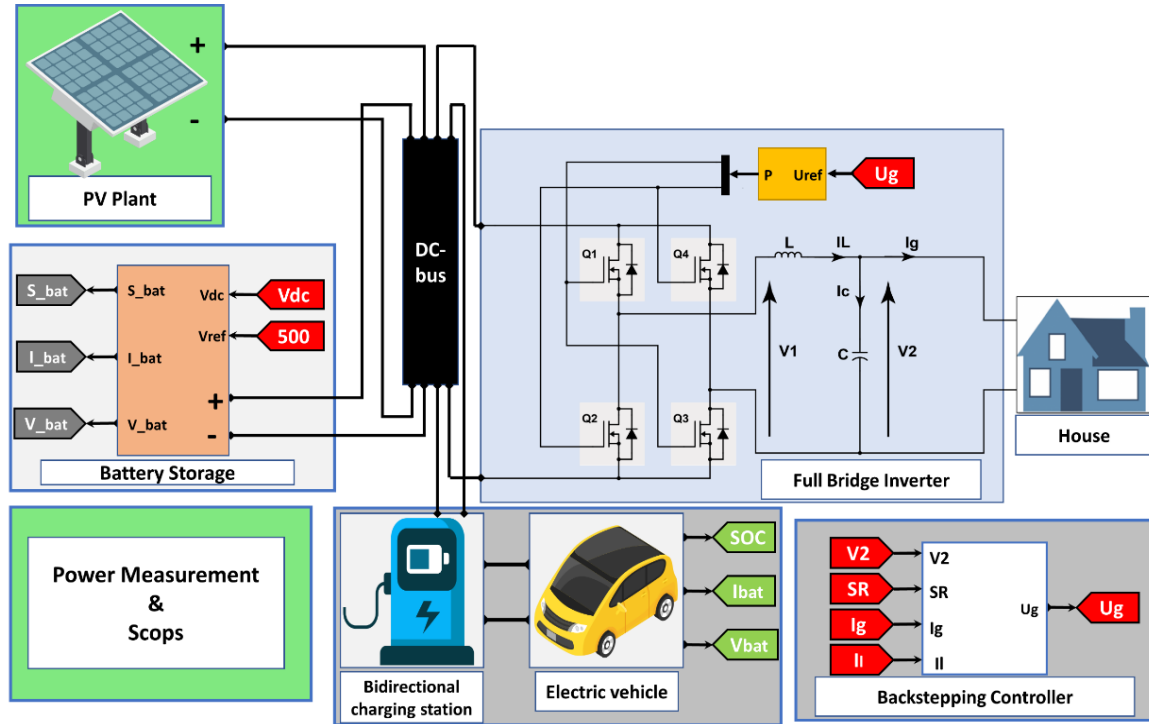
Figure 4. Simulation setup

Table 1. Simulation parameters

Parameter	Value	Parameter	Value
L	5 mH	V_2	220 V
C	100 μF	$Load_1$	2 KW
C-bus	12000 μF	$Load_2$	4 KW
f	50 Hz	$Load_3$	6 KW
F_{sw}	20 KHz	$μ_1$	100
V_{DC}	500 V	$μ_2$	100
EV battery capacity	40 kWh	$λ_{1,2,3}$	3

In Figure 6, the inverter's output voltage using the Backstepping controller is compared to that of the same inverter controlled by the conventional proportional-integral-derivative (PID). Based on the obtained results it is clear that the backstepping voltage represented by the solid blue line converges towards the reference voltage given by the red plus pattern in just $10^{-3}(s)$. Which substantiates the tracking performances of the adopted control scheme. Furthermore, compared to the PID voltage given in the dotted green line, the backstepping voltage is clearly more stable since it does not present any oscillations. It rather maintains a sinusoidal form of 50 Hz frequency and 220 V amplitude throughout the entirety of the simulations, which is crucial for the household electrical equipment. With regards to the quality of the output power, Figure 7 shows that the power provided to the house under a constant load is stable with no fluctuations, which is a critical requirement for power systems especially if there is no electric grid to smoothen the power.

Being that the daily power demand of most houses varies depending on the number of connected equipment, in this section, the robustness of the adopted control schemes is evaluated under a load variation scenario. For this purpose, the power profile in Figure 8 is adopted. This latter simulates instantaneous transitions between three load values; $P_1 = 2\,KW$, $P_2 = 4\,KW$, and $P_3 = 6\,KW$. The obtained results are illustrated in Figures 9 and 10.

As illustrated, in Figures 9 and 10, the sequence of sudden variations in power demand has no effect on the performance of the controllers. In this regard, Figure 9 shows that the output voltage's amplitude and frequency are successfully maintained at 220 V and 50 Hz respectively regardless of the load variations. This is showcased in the zoomed area of Figure 9. Concurrently, the amplitude of the electrical current in Figure 10, varies in accordance with the load to satisfy the power requirement, while maintaining a perfect sinusoidal form of 50 Hz frequency as shown in the zoomed area. The quality of the inverter's output signals

is further validated by a frequency analysis conducted on the voltage supplied to the loads as presented in Figure 11. The analysis yielded a THD of about 0.25%, which is below the acceptable range (5%) according to the standard of IEEE-519 (IEEE 519 working group, 1992).
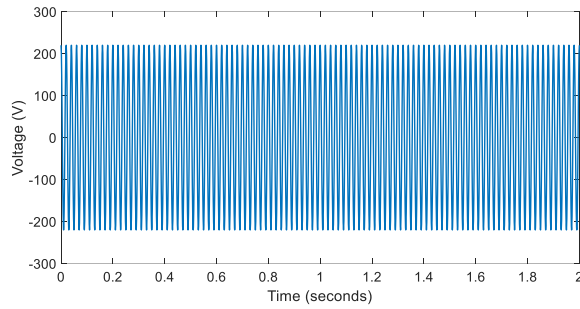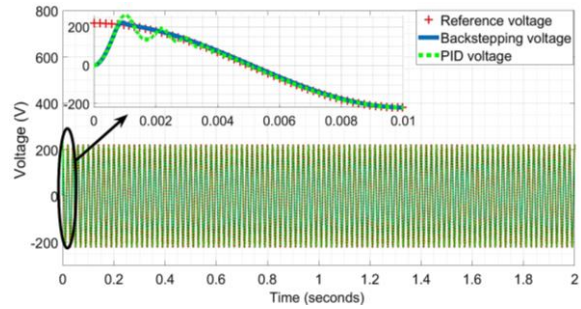

Figure 5. Reference voltage signal

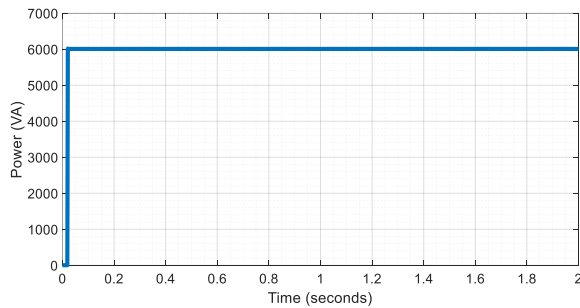Figure 6. The output voltage of the power inverter
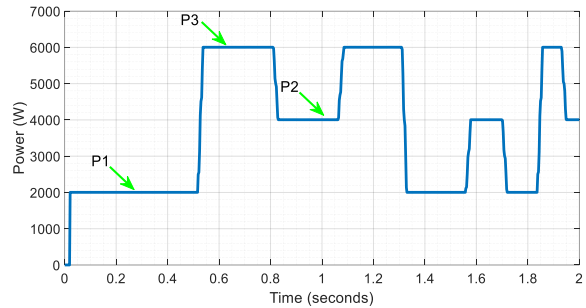

Figure 7. Output power provided to the house
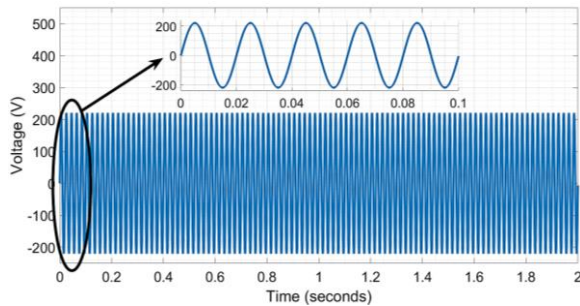

Figure 8. The output power of the inverter

Figure 9. The output voltage of the inverter
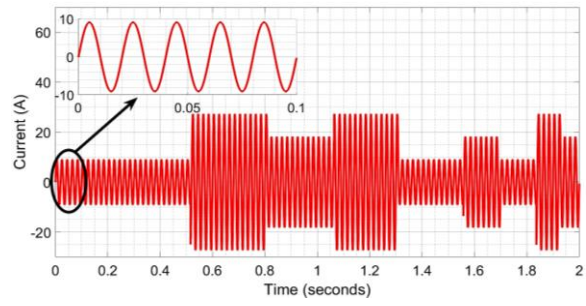
Figure 10. The load's current variation
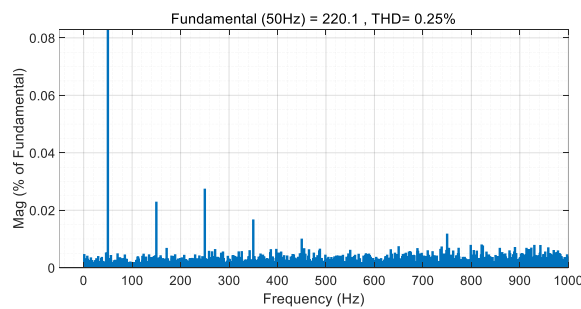
Figure 11. Analysis of THD of the output voltage

4. CONCLUSION

In this paper, the power transfer between an EV and an isolated house was controlled using an adaptive backstepping approach and an integral sliding mode scheme within the framework of vehicle-to-house technology. The robustness of both controllers was investigated under both fixed and variable load scenarios and resulted in satisfactory performances. In this regard, the output signal of the inverter follows with great accuracy the reference signal, resulting in a perfect sinusoidal waveform. This is supported by the frequency analysis of the output signal, which yielded a THD value of 0.25% total harmonic distortion. As a result, the authors recommend these two control strategies for vehicle-to-house technology.

REFERENCES

[1]   S.-C. Ma, J.-H. Xu, and Y. Fan, "Characteristics and key trends of global electric vehicle technology development: A multi-method patent analysis," *Journal of Cleaner Production*, vol. 338, Mar. 2022, doi: 10.1016/j.jclepro.2022.130502.
[2]   D. Liu, L. Xu, U. H. Sadia, and H. Wang, "Evaluating the CO2 emission reduction effect of China's battery electric vehicle promotion efforts," *Atmospheric Pollution Research*, vol. 12, no. 7, Jul. 2021, doi: 10.1016/j.apr.2021.101115.
[3]   A.-M. Hariri, M. A. Hejazi, and H. Hashemi-Dezaki, "Investigation of impacts of plug-in hybrid electric vehicles' stochastic characteristics modeling on smart grid reliability under different charging scenarios," *Journal of Cleaner Production*, vol. 287, Mar. 2021, doi: 10.1016/j.jclepro.2020.125500.
[4]   S. S. Ravi and M. Aziz, "Utilization of electric vehicles for vehicle-to-grid services: progress and perspectives," *Energies*, vol. 15, no. 2, Jan. 2022, doi: 10.3390/en15020589.
[5]   P. Sharma, S. Reddy Salkuti, and S.-C. Kim, "Advancements in energy storage technologies for smart grid development," *International Journal of Electrical and Computer Engineering (IJECE)*, vol. 12, no. 4, pp. 3421–3429, Aug. 2022, doi: 10.11591/ijece.v12i4.pp3421-3429.
[6]   S. Rafique, M. J. Hossain, M. S. H. Nizami, U. Bin Irshad, and S. C. Mukhopadhyay, "Energy management systems for residential buildings with electric vehicles and distributed energy resources," *IEEE Access*, vol. 9, pp. 46997–47007, 2021, doi: 10.1109/ACCESS.2021.3067950.
[7]   H. B. Sassi, C. Alaoui, F. Errahimi, and N. Es-Sbai, "Vehicle-to-grid technology and its suitability for the Moroccan national grid," *Journal of Energy Storage*, vol. 33, Jan. 2021, doi: 10.1016/j.est.2020.102023.
[8]   N. Hinov, V. Dimitrov, and G. Vacheva, "Model for vehicle to home system with additional energy storage for households," *Electronics*, vol. 10, no. 9, May 2021, doi: 10.3390/electronics10091085.
[9]   Y. Mazzi, H. B. Sassi, F. Errahimi, and N. Es-Sbai, "State of charge estimation using extended Kalman filter," in *2019 International Conference on Wireless Technologies, Embedded and Intelligent Systems (WITS)*, Apr. 2019, pp. 1–6, doi: 10.1109/WITS.2019.8723707.
[10]   P. K. Gayen, P. Roy Chowdhury, and P. K. Dhara, "An improved dynamic performance of bidirectional SEPIC-Zeta converter based battery energy storage system using adaptive sliding mode control technique," *Electric Power Systems Research*, vol. 160, pp. 348–361, Jul. 2018, doi: 10.1016/j.epsr.2018.03.016.
[11]   D. Marinho, M. Chaves, P. Gambôa, and J. Lopes, "Conversion system for grid-to-vehicle and vehicle-to-grid applications," *Journal of Electrochemical Energy Conversion and Storage*, vol. 17, no. 1, Feb. 2020, doi: 10.1115/1.4043538.
[12]   F. Mendez-Diaz, B. Pico, E. Vidal-Idiarte, J. Calvente, and R. Giral, "HM/PWM seamless control of a bidirectional buck-boost converter for a photovoltaic application," *IEEE Transactions on Power Electronics*, vol. 34, no. 3, pp. 2887–2899, Mar. 2019, doi: 10.1109/TPEL.2018.2843393.
[13]   Y. M. Alsmadi, V. Utkin, and L. Xu, "Sliding mode control design procedure for power electronic converters used in energy conversion systems," in *New Perspectives and Applications of Modern Control Theory*, Cham: Springer International Publishing, 2018, pp. 465–521.
[14]   S. Das, M. S. Qureshi, and P. Swarnkar, "Design of integral sliding mode control for DC-DC converters," *Materials Today: Proceedings*, vol. 5, no. 2, pp. 4290–4298, 2018, doi: 10.1016/j.matpr.2017.11.694.
[15]   M. Riaz, A. R. Yasin, A. Arshad Uppal, and A. Yasin, "A novel dynamic integral sliding mode control for power electronic converters," *Science Progress*, vol. 104, no. 4, Oct. 2021, doi: 10.1177/00368504211044848.
[16]   M. Facta, A. Priyadi, and M. H. Purnomo, "Investigation of symmetrical optimum PI controller based on plant and feedback linearization in grid-tie inverter systems," *International Journal of Renewable Energy Research*, 2017, doi: 10.20508/ijrer.v7i3.5984.g7188.
[17]   S. Ghosh, B. Moulik, and H. P. Singh, "Coordinated converter-inverter PI based grid tied photovoltaic system," in *2021 6th International Conference for Convergence in Technology (I2CT)*, Apr. 2021, pp. 1–7, doi: 10.1109/I2CT51068.2021.9418065.
[18]   J. A. Cortajarena, O. Barambones, P. Alkorta, and J. De Marcos, "Sliding mode control of grid-tied single-phase inverter in a photovoltaic MPPT application," *Solar Energy*, vol. 155, pp. 793–804, Oct. 2017, doi: 10.1016/j.solener.2017.07.029.
[19]   G. V. Hollweg, P. J. D. de Oliveira Evald, E. Mattos, R. V. Tambara, and H. A. Gründling, "Feasibility assessment of adaptive sliding mode controllers for grid-tied inverters with LCL filter," *Journal of Control, Automation and Electrical Systems*, vol. 33, no. 2, pp. 434–447, Apr. 2022, doi: 10.1007/s40313-021-00835-5.
[20]   A. K. Zadeh, L. I. Kashkooli, and S. A. Mirzaee, "Designing a power inverter and comparing back-stepping, sliding-mode and fuzzy controllers for a single-phase inverter in an emergency power supply," *Ciência e Natura*, vol. 37, Dec. 2015, doi: 10.5902/2179460X20769.
[21]   S. Salimin, S. A. Zulkifli, and M. Armstrong, "Reduction in current THD of grid parallel inverters using randomized PR control," *International Journal of Power Electronics and Drive Systems (IJPEDS)*, vol. 8, no. 1, pp. 290–296, Mar. 2017, doi: 10.11591/ijpeds.v8.i1.pp290-296.
[22]   R. Majdoul, A. Touati, A. Ouchatti, A. Taouni, and E. Abdelmounim, "Comparison of backstepping, sliding mode and PID regulators for a voltage inverter," *International Journal of Electrical and Computer Engineering (IJECE)*, vol. 12, no. 1,

pp. 166–178, Feb. 2022, doi: 10.11591/ijece.v12i1.pp166-178.

[23] H. B. Sassi, F. Errahimi, N. Es-Sbai, and C. Alaoui, "Comparative study of ANN/KF for on-board SOC estimation for vehicular applications," *Journal of Energy Storage*, vol. 25, Oct. 2019, doi: 10.1016/j.est.2019.100822.

[24] Y. Mazzi, H. Ben Sassi, A. Gaga, and F. Errahimi, "State of charge estimation of an electric vehicle's battery using tiny neural network embedded on small microcontroller units," *International Journal of Energy Research*, vol. 46, no. 6, pp. 8102–8119, May 2022, doi: 10.1002/er.7713.

[25] V. Utkin, "Variable structure systems with sliding modes," *IEEE Transactions on Automatic Control*, vol. 22, no. 2, pp. 212–222, Apr. 1977, doi: 10.1109/TAC.1977.1101446.

[26] A. Bessas, A. Benalia, and F. Boudjema, "Integral sliding mode control for trajectory tracking of wheeled mobile robot in presence of uncertainties," *Journal of Control Science and Engineering*, pp. 1–10, 2016, doi: 10.1155/2016/7915375.

[27] M. Idrees, S. Ullah, and S. Muhammad, "Sliding mode control design for stabilization of underactuated mechanical systems," *Advances in Mechanical Engineering*, vol. 11, no. 5, May 2019, doi: 10.1177/1687814019842712.

[28] S. Adak, "Harmonics mitigation of stand-alone photovoltaic system using LC passive filter," *Journal of Electrical Engineering and Technology*, vol. 16, no. 5, pp. 2389–2396, Sep. 2021, doi: 10.1007/s42835-021-00777-7.

BIOGRAPHIES OF AUTHORS

Hicham Ben Sassi is professor at the Private University of Fez, Morocco. He received his Ph.D in Electrical Engineering from the University of Sidi Mohammed Ben Abdellah, Faculty of Science and Technologies, Morocco. His research interests include, electric vehicles, batteries, renewable energy, power electronics and artificial intelligence. He can be contacted at email: hicham.1bensassi@gmail.com.

Yahia Mazzi received the M.S. degree in Electronic, Signals, and Automated Systems from the Faculty of Sciences and Technologies of Fez, Sidi Mohamed Ben Abdellah University, Morocco, in 2018. He is currently pursuing a Ph.D. degree in Energy Management for Electric Vehicles at the Laboratory of Intelligent Systems, Georesources and Renewable Energies (LISGRE ISGRE). His research interests include electric vehicles, batteries, battery management system, electric vehicle motor drive control, renewable energies, power electronics, embedded systems, and the application of artificial intelligence in power system and EV battery management system. He can be contacted at: yahia.mazzi@usmba.ac.ma.

Fatima Errahimi is teacher and researcher at the Faculty of Sciences and Technologies in Sidi Mohamed Ben Abedellah University of Fez. She got Ph.D degree on Automatic Control System and robotics in 2004. Her special fields of interest include the integration of renewable energy sources in building energy management, optimization control for demand side units in households and smart grid. She participated in many research projects among which the IRESEN one on low cost CPV in Morocco. She supervised many Ph.D thesis and several post graduate students. She can be contacted at: fatima.errahimi@usmba.ac.ma.

Najia Es-Sbai received her Ph.D. degree from Pau University (France) in 1993. She is a Professor in the Electric Engineering Department at the Faculty of Science and Technology, University of Sidi Mohamed Ben Abdellah (USMBA-Fez Morocco), since 1995. She completed her Ph.D. (doctorat d'état) at USMBA in 2002. She was deputy head of the electrical engineering department at the Faculty of Science and Technology of Fez for the period 2010-2013. Her main research concerns area of nanostructures. In recent years, she focused on image processing, especially emotions detection and renewable energy. She is member and Deputy Director of the Laboratory of Intelligent Systems, Georesources and Renewable Energies (LISGRE) since 2014 and she is concerning in supervising many Ph.D. thesis. Theses concerning the management and optimization of energy flows in a smart grid DC isolated, intelligent inverter, DC-DC converters for energy optimization, and facial expression emotion detection. She can be contacted at email: najia.essbai@usmba.ac.ma.